J Solid State Electrochem (2012) 16:3267–3274
DOI 10.1007/s10008-012-1765-9

ORIGINAL PAPER

Deposition and characterization of $BiVO_4$ thin films and evaluation as photoanodes for methylene blue degradation

M. R. da Silva · L. H. Dall'Antonia · L. V. A. Scalvi · D. I. dos Santos · L. O. Ruggiero · A. Urbano

Received: 1 March 2012 / Revised: 27 April 2012 / Accepted: 28 April 2012 / Published online: 17 May 2012

Abstract Thin films of bismuth vanadate ($BiVO_4$) are deposited through the solution combustion synthesis technique coupled with the dip-coating process. Thermal gravimetric analyis shows a total mass loss of 71 % besides the formation of the monoclinic phase, about 300 °C, which is also revealed by X-ray diffraction. UV–Vis optical absorption spectra show direct bandgap transition about 2.5 eV for films, in good agreement with semiconducting monoclinic phase. Scanning electron microscopic images reveal that thermal annealing time at 500 °C is a very important parameter to control the thickness and shape of the particles and yields an average thickness of about 800 nm for 10 dip-coated deposited layers, with round-shaped nanometric-sized particles, homogeneously distributed on the film surface. Photoelectrochemical degradation of methylene blue by a bismuth vanadate film deposited on fluor-doped tin oxide substrate shows up as a very efficient process. The first-order rate constant for the photoinduced process is about five times the rate constant for degradation in the dark, showing the capacity of the $BiVO_4$/fluorine-doped tin oxide film for electrochemical degradation, mainly in the presence of light.

Keywords Semiconductors · Chemical synthesis · Thermogravimetric analyis (TGA) · X-ray diffraction · Electrochemical properties

M. R. da Silva
Engineering College, CTI,
UNESP—State University of São Paulo,
Bauru, SP, Brazil

M. R. da Silva
POSMAT—Programa de Pós Graduação em Ciência e Tecnologia de Materiais, FC, UNESP—State University of São Paulo,
Bauru, SP, Brazil

L. H. Dall'Antonia
Department of Chemistry, UEL—State University of Londrina,
Londrina, PR, Brazil

L. V. A. Scalvi (✉) · D. I. dos Santos · L. O. Ruggiero
Department of Physics, FC,
UNESP—State University of São Paulo,
Bauru, SP, Brazil
e-mail: scalvi@fc.unesp.br

A. Urbano
Department of Physics, UEL—State University of Londrina,
Londrina, PR, Brazil

L. V. A. Scalvi
Meteorological Research Institute,
UNESP—State University of São Paulo,
Bauru, SP, Brazil

Introduction

In recent years, seeking for sustainability has become the rule for government institutions all over the world. Allied to this concept, the ambient preservation is a fundamental part of a modern world, leading the scientific community to search solutions to minimize the impact caused by technological society. In this direction, photocatalytic materials have earned deep investigation because they may be used in a wide range of ambient applications, such as water purification and residual water treatment [1–3], besides clean energy generation [4]. Among the investigated materials for this goal, the semiconductor bismuth vanadate ($BiVO_4$) has received special attention, due to its photocatalytic activity in the degradation of organic compounds and dyes in aqueous media, when irradiated with $\lambda \leq 520$ nm [5–8], besides allowing the partial break of water molecule for oxygen generation, when irradiated with visible light [9, 10]. This semiconductor material also presents other interesting properties such as: ferroelasticity [11], ionic conductivity [12], and photochromism [13].

The electronic structure of $BiVO_4$ is still a matter of controversy, mainly concerning the direct or indirect transition. Most recently, Walsh and coworkers [14] have investigated the electronic structure through first principles calculation and have concluded that $BiVO_4$ is a direct bandgap semiconductor due to the presence of empty 3*d* orbital of vanadium coupled to orbitals 2*p* of oxygen and 6*p* of bismuth, resulting in a conduction band minimum at the Brillouin zone edge, favorable to low-energy direct transition. This semiconductor compound may exist in three distinct polymorphic phases, namely tetragonal zircon structure, monoclinic scheelite structure, and tetragonal scheelite structure [15]. The monoclinic phase presents higher photocatalytic activity when compared to the other two phases [16], which is related to the narrower bandgap value, 2.4 eV, unlike the tetragonal phase value, 3.1 eV. This smaller bandgap value allows its application in the photocatalysis in wider spectra, from visible to the ultraviolet range [17]. There are few methods for the synthesis of bismuth vanadate, such as solid state reaction [18], hydrothermal synthesis [19, 20], sonochemical method [21], coprecipitation in aqueous media [22, 23], electrochemical synthesis [24], sol–gel [25], and solution combustion synthesis (SCS) [26]. Among all of these processes, the SCS process may be selected due to its simplicity and versatility for the obtaining $BiVO_4$ nanocrystals with monoclinic structure and relatively low cost [10, 22]. Several authors have reported the utilization of SCS method for achieving the $BiVO_4$ monoclinic phase with specific application in heterogeneous catalysis [23, 24]. For instance, Jiang and coworkers [23] have synthesized nanocrystals of $BiVO_4$ in the monoclinic phase, used for degradation of methylene blue in aqueous media with high efficiency. Zhou and coworkers [24] reported the photoactivity of the composite Co–$BiVO_4$ for the degradation of methylene blue under irradiation with visible light. Their results show that a composite with 5 % of Co in the $BiVO_4$ matrix leads to degradation of 90 % of the initial concentration of methylene blue.

Although these papers show the application of this semiconductor compound for the photocatalytic use, for practical purposes, the shape of the sample must be adequately chosen. Thin films of $BiVO_4$ seem to be a good option [27] and several authors report the use of $BiVO_4$ thin films in heterogeneous photocatalysis [3, 15, 27, 28]. Xie and coworkers [3] synthesized $BiVO_4$ thin films with monoclinic structure via chemical synthesis using the citrate route, for acid Orange 7 degradation under visible light irradiation. The results show that in 3 h, the film presents 78.9 % of efficiency and durability for repeated experiments. Zhou and coworkers [15] synthesized $BiVO_4$ thin films with monoclinic structure via dip coating, for degradation of 2,4-dichlorophenol and bisphenol, also under visible light irradiation. In this case, 90 % of organic pollutants were removed in 5 h, with high photocatalytic efficiency. The thin film operation is also fundamental, where photoelectrocatalytic processes present some advantages compared to photocatalytic processes. In the first case, the applied potential to the electrochemical system forces the photogenerated charge carriers towards the electrode, avoiding the electron hole recombination, unlike the simply photocatalytic process [27].

The present report proposes the $BiVO_4$ synthesis by the SCS method, coupled to thin film deposition by the dip-coating technique. The material is characterized by thermal analysis [differential thermal analysis–thermogravimetric analysis (DTA–TGA)], X-ray diffraction (XRD), and scanning electron microscopy (SEM). Optical characterization through UV–Vis absorption is also carried out, in order to verify the optical transparency and evaluate the material bandgap. Photoelectrochemical analysis is done by linear voltammetry and chronoamperometry with visible light irradiation. The degradation of methylene blue is investigated in the dark and under irradiation with visible light, using $BiVO_4$ thin film deposited on fluorine-doped tin oxide (FTO) substrates ($BiVO_4$/FTO electrode).

Experimental

Synthesis of $BiVO_4$ thin film

The $BiVO_4$ solution is obtained through the SCS technique. Firstly, 0.48 g of citric acid (Sigma-Aldrich, PA) and 1.21 g of $Bi(NO_3)_3{\cdot}5H_2O$ (Sigma-Aldrich, PA) are dissolved in 50 mL of HNO_3 (Merck, PA) 1.5 mol L^{-1}. Concentrated NH_4OH (Merck, PA) is added to this solution very slowly until the pH reaches 7. This procedure is followed by the addition of 1 g of urea (Sigma-Aldrich, PA), giving birth to a transparent solution. In another recipient, 0.48 g of citric acid and 0.29 g of NH_4VO_3 (Sigma-Aldrich, PA) are dissolved by 50 mL of deionized water, previously heated to 70 °C, under constant agitation with a magnetic bar for 30 min, producing a yellowish solution. Both solutions were mixed and placed in an oven at 80 °C, remaining in this temperature for 20 h. The final product is a green gel, due to the combustion in solution. This gel is diluted in 50 mL of deionized water, becoming a lighter green solution, named here as "work" solution. For the thin film deposition, the dip-coating technique is used, where the dipping process is carried out into the work solution, with a dipping rate of 10 cm min^{-1}. After each dipping process, the sample is fired at 400 °C for 10 min in air. A total of 10 layers were deposited and a final thermal annealing at 500 °C by 1 h took place. For most of the analyses, the used substrate is soda–lime glass from Corning, except for the photoelectrochemical analysis, where an FTO conductor electrode is provided.

Thin film characterization

XRD measurements, in the shallow angle configuration, were carried out using a PANalytical diffractometer, model X'Pert

PRO MPD, with the CuK_α (1.5418 Å) radiation, coupled to a nickel filter, in order to eliminate the CuK_β radiation. The applied tension was 40 kV and the current was 30 mA. The scanning range was from 10° to 80°, with regular step of $0.05° s^{-1}$. SEM images were obtained in a Quanta 200-FEI microscope with 30 kV of applied voltage. Simultaneous thermal analyses (DTA/TGA) have been performed in a STA 409 NETZSCH system. The original material, in the form of green gel (prior to the dilution in water for thin film deposition) is placed in an alumina crucible, and an empty alumina crucible is used as reference. Both crucibles were submitted to a heating process with rate of 10 °C min^{-1} under dynamic atmosphere of N_2. For the evaluation of the optical properties, optical absorption spectra were taken in the UV–Vis, range 190–900 nm, with Cary 1G equipment.

Photoelectrochemical measurements

Conventional three electrodes were used for the photoelectrochemical experiments, where an Ag/AgCl (1 mol L^{-1} KCl) electrode is the reference, a platinum wire (10 cm in length and 0.5 mm in diameter) is the counter-electrode, and the $BiVO_4$ thin film, deposited on FTO conductor substrate, is the work electrode (the geometrical electrode area in contact with the solution is set to 1 cm^2). The light irradiation in the electrochemical system is done through a Philips dichroic lamp with a power of 50 W at an applied voltage of 12 V; this light source presents wide spectra from $\lambda \geq 400$ nm. It must be mentioned that illumination was done on the $BiVO_4$ surface, in the front part of the electrode system. The photoelectrochemical profile of the $BiVO_4$ film was obtained with the linear voltammetry technique, through a potentiostat/galvanostat AUTOLAB 84057, version 4.9, using 5 mL of KCl and Na_2SO_4 solution (both 0.1 mol L^{-1} concentrated) as electrolytes and at scanning rate of 5 mV s^{-1}, in the range 0–1.4 V.

For the 5 mL (10 μmol L^{-1}) methylene blue electro- and photoelectrochemical degradation, in Na_2SO_4 0.1 mol L^{-1} electrolyte, the chronoamperometry technique was used, with controlled potential of 1.4 V during different degradation times. The 1.4-V bias was chosen because this value leads to the highest photogenerated current, as will be shown in the next section. Then, it allows efficient methylene blue degradation. The photoelectrochemical degradation was carried out submitting to visible light irradiation from the Philips lamp, whereas the electrochemical degradation was done in the dark conditions. After degradation, UV–Vis spectra of the remaining solution were taken and used to verify the relative (percentage) amount of methylene blue that had vanished. The adopted parameter was the decreasing of the methylene blue optical absorption band, taken at approximately 665 nm. These spectra were taken just after the chronoamperometry measurements.

Results and discussion

Morphology and structure of $BiVO_4$ thin films

DTA and TGA curves were obtained from the green $BiVO_4$ gel (prior to the dilution) and are shown in Fig. 1. A total mass loss of 71 % was observed, occurring in several steps related to physical and chemical processes occurring along with the heating up to 350 °C. The first endothermic peak, in the region below 120 °C, is associated to the elimination of free and adsorbed water. The next events are underlined by the first hachured region and include the range between 122 and 170 °C, where two exothermic peaks are observed and are probably related to urea decomposition [29]. In the next hachured region, two distinct exothermic events are taking place. The first and more intense peak corresponds to the decomposition of distinct nitrates, including ammonia nitrate, which is accompanied with significant mass loss and has a maximum in about 270 °C. The other exothermic peak is evidenced from approximately 287 °C and has a maximum at about 350 °C, which is related to decomposition and combustion of citrates [29] and, besides, can also be associated with the formation of monoclinic phase of $BiVO_4$ [22, 30, 31]. The endothermic peak at 927 °C is related to the fusion of $BiVO_4$ [32]. DTA–TGA results yield important information towards the obtaining of monoclinic phase of $BiVO_4$, mainly the adequate temperature for sample thermal annealing, which in the case of the green gel is in the range 300–350 °C. Based on these results, the temperature of 400 °C was chosen for the intermediate thermal annealing of film layers and 500 °C was chosen for the final thermal annealing, in order to assure the formation of the monoclinic phase of $BiVO_4$ as the dominant one in the films. The presence of the monoclinic crystalline phase was confirmed by X-ray diffraction results as discussed below. The results obtained in this paper, concerning the DTA–TGA analysis, are in good agreement with previously published reports [30, 31]. For instance, the synthesis of $BiVO_4$ nanocrystals by the SCS technique using sodium carboxymethyl

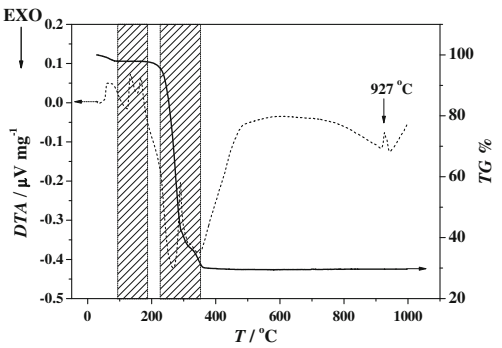

Fig. 1 DTA–TGA curve of the precursor gel

cellulose as combustible and stabilizing agent [31] also leads to $BiVO_4$ monoclinic phase formed in the range 200–300 °C.

Figure 2 shows X-ray diffractograms of the green gel, treated at different temperatures (Fig. 2a) and of the $BiVO_4$ thin film deposited on FTO-conducting substrate (Fig. 2b), where the deposited film has 10 layers and final thermal annealing was carried out at 500 °C by 1 h. These diffractograms present rather noisy profile and broad peaks, which is typical of materials of nanocrystallized domain. Results shown in Fig. 2a suggest that for calcination temperatures of 150 and 200 °C, samples are composed of a phase mixture. Diffraction peaks at 17.6°, 30.7°, and 35.9° are probably related to the orthorhombic phase of V_2O_5 (PDF 85–2,422) and peaks at 22.5°, 32.9°, are 37.8° may come from tetragonal β-Bi_4O_7 (PDF 74–2,352). From 300 °C, the indexed peaks are associated mainly with the plans of the monoclinic structure of $BiVO_4$, with space group *I2/b*. According to the file PDF 75–1,867 from the software PCPDFWIN, version 2.4, JCPDS-ICDD, the lattice parameters are: a=5.195 Å, b=5.093 Å, and c=11.704 Å. For the film diffractogram (Fig. 2b), besides the monoclinic $BiVO_4$, it is also possible to observe the diffraction peaks from the FTO substrate, as also shown in the lower curve of Fig. 2b.

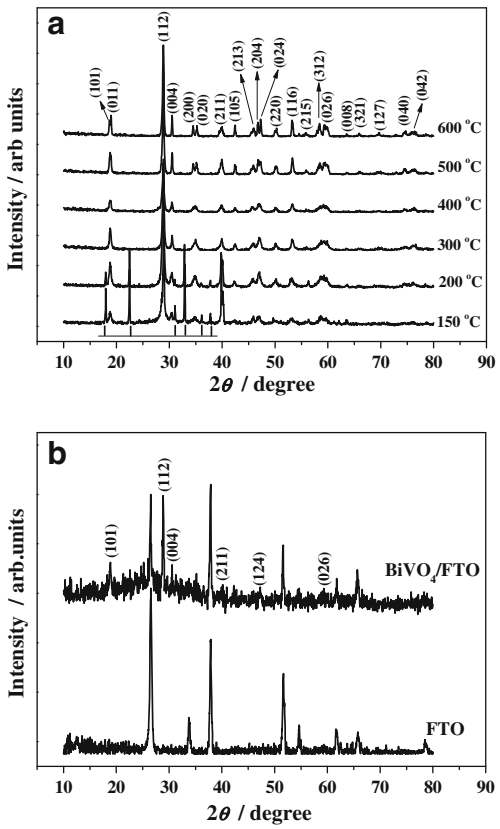

Fig. 2 **a** X-ray diffractograms of the green gel, treated at different temperatures. **b** X-ray diffractogram of $BiVO_4$ thin film with 10 layers, deposited on FTO substrate and annealed at 500 °C by 1 h

It is important to mention that X-ray diffraction data of films deposited in soda–lime glass were omitted in Fig. 2b, but they yield diffractograms quite similarly, except for the absence of FTO substrate characteristic peaks, due to the amorphous structure of this sort of substrate. An estimation of the crystallite average size was calculated using the Scherrer equation [33], for the most intense $BiVO_4$ peak, located at 29.0° and associated with the plan (112), yielding an average size of 34 nm. The X-ray results shown here are in good agreement with other combined processes for obtaining $BiVO_4$ [7, 17, 34, 35].

SEM image seen in subpanels a and b of Fig. 3 shows topographic and cross-section image, respectively, of a $BiVO_4$ film with 10 layers thermally annealed at 500 °C by 1 h. Figure 3a shows a quite homogeneous surface with round-shaped particles homogeneously distributed throughout the investigated area, and Fig. 3b shows a rather uniform thickness of the film. These particles evaluated from the surface picture, using the magnification bar, yield an average grain size of about 350 nm, while the crystallite size determined through the Scherrer equation is about 34 nm, as mentioned previously. Then, a fair assumption is that these particles, seen in the SEM image, are composed of smaller unities, the monoclinic $BiVO_4$ crystallites. The film thickness, evaluated the film cross section, seen in Fig. 3b is about 800 nm. Figure 3c, d show results for films with 10 layers and annealing temperature of 500 °C for 6 h. It is clearly observed that the thermal annealing time is a very relevant parameter for film homogeneity and morphology. SEM picture allows inferring that a sintering process may have taken place and a grain growth has occurred. In this case, there is basically a bimodal distribution of particles: a distribution around 1.0 μm size and another around 500 nm. Besides, some voids between grains are observed, though where it is possible to see the substrate surface. The cross-section image, Fig. 3d, reveals a quite nonuniform film. These images suggest that a long thermal annealing is not recommended for this thin film deposition process. Similar SEM images can be found in the literature. Zhang and coworkers [27] synthesize $BiVO_4$ films by modified metal-organic decomposition technique coupled with spin-coating process on FTO substrate. Although this process is completely different from the techniques used here, the deposited film also presents good homogeneity of round-shaped particle dispersion on the substrate. Moreover, $BiVO_4$ powder has been obtained with nanometric dimensions such as nanoribbons [36], nanospheres [17, 29], dendrite crystals [37], and other similar shapes. Textured films are very attractive because, like nanoribbons and nanowires, they would open the possibility of very low electron scattering in electrical transport processes. Consequently, optimization of the final thermal annealing should be the next step in order to improve the alignment of the surface nanoparticles.

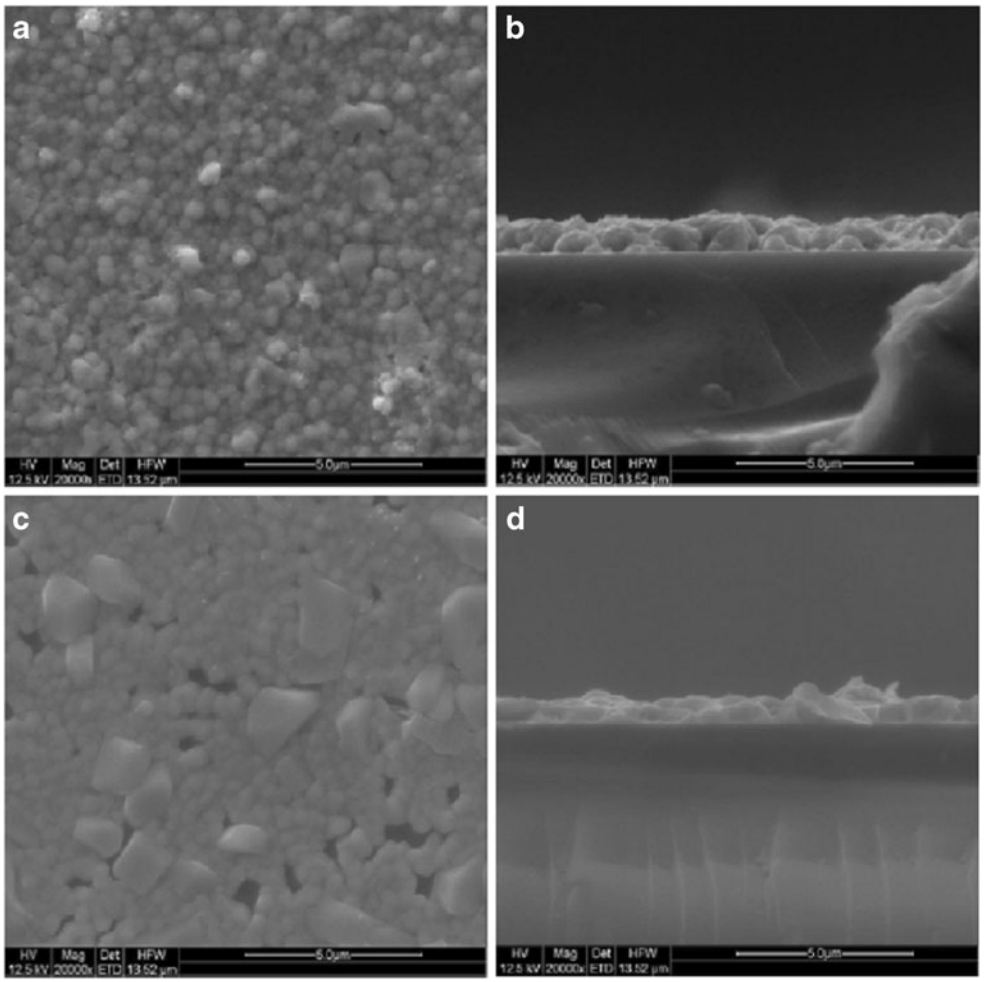

Fig. 3 SEM images of $BiVO_4$ thin film. **a** Surface and **b** cross-section images of thin film thermally annealed at 500 °C by 1 h and **c** surface and **d** cross-section images of thin film thermally annealed at 500 °C by 6 h

Optical characterization and bandgap evaluation of $BiVO_4$ thin films

UV–Vis optical absorption data, recorded for the thin films, are shown in Fig. 4, along with the bandgap evaluation seen in the inset. The fundamental absorption edge starts at about 527 nm as seen by the extrapolation (dotted line) of the absorption spectra. Considering the bandgap transition nature as direct [14], the value of the bandgap for this film can be evaluated, in good approximation, by the $(\alpha h\upsilon)^2$ vs. $(h\upsilon)$ plot and the crossing of the slope of the linear part with the "x" axis [21, 38]. The obtained result, shown in the inset of Fig. 4, yields a bandgap value of about 2.5 eV, typical of $BiVO_4$ monoclinic phase, and in good agreement with published reports for thin films obtained by other techniques [3, 15, 27, 28, 30] as well as nanocrystalline powders [7, 22, 26, 29].

$BiVO_4$ thin film photoelectrochemical characterization

The photoelectrochemical behavior of the $BiVO_4$ thin film, deposited on FTO substrate, was evaluated through linear voltammetry with chopped (5 min long pulse) visible light ($\lambda \geq 400$ nm), which generates both the dark current and the photocurrent during a single linear sweep. One must recall that light irradiation was directed to $BiVO_4$ film surface, in the front part of the electrode system, since illumination in the back may lead to distinct results. The result is presented in Fig. 5 and shows that the sensibility of investigated film to visible light, where a current jumps under light irradiation is

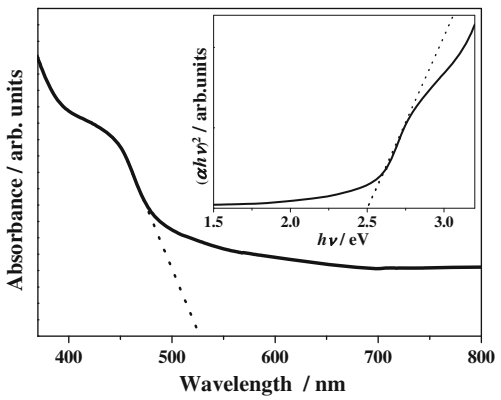

Fig. 4 UV–Vis optical absorption spectra of $BiVO_4$ thin film. *Inset*: direct bandgap evaluation

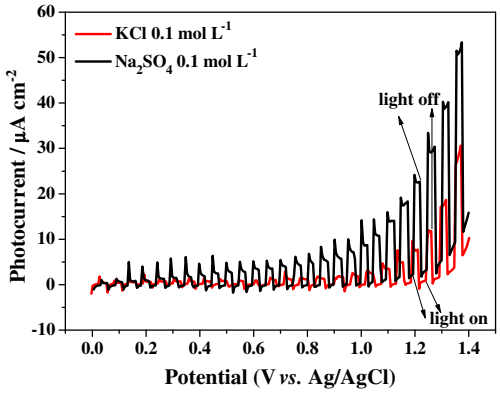

Fig. 5 Linear voltammetry of $BiVO_4$ thin film in the presence of pulsed visible light in KCl and Na_2SO_4 electrolytes, both 0.1 mol L^{-1}, v=5 mV s^{-1}

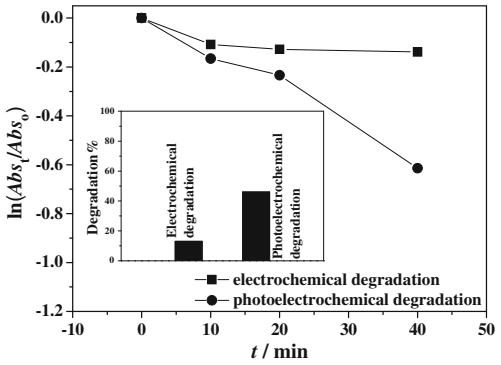

Fig. 7 Decrease of methylene blue concentration after electrochemical or photoelectrochemical degradation by $BiVO_4$/FTO thin film. The *lines* represent only a guide for the eyes. *Inset*: degradation percentage at 40 min of reaction

observed, which decays when the illumination is removed. This effect of visible light irradiation is related to the light energy range, with values above the $BiVO_4$ bandgap (about 2.5 eV), promoting electrons from the valence band (orbital Bi 6*s*) to the conduction band (orbital V 3*d*), leading to an electrical current increase, due to generation of higher amount of charge carriers [21]. The increasing anodic photocurrent with increasing positive potential indicates n-type semiconductor behavior. It can be related with electron migration to the FTO contact and holes to the $BiVO_4$ film surface, in order to oxidize water at the interface electrode/solution through $OH^{\bullet}$ radicals, which play a fundamental role in the methylene blue degradation, more specifically on the compound discoloration, related to the attack to the molecule chromophore group [11]. The curves exhibit distinct differences upon changing the potential sweep direction (results not shown). Besides, the photoresponse is strongly influenced by the sort of used electrolyte. In the Na_2SO_4, 0.1 mol L^{-1}, the current is higher than in the KCl electrolyte, in the same concentration, all over the potential window used (0–1.4 V vs. Ag/AgCl). At about 1.37 V, the photoinduced current observed for the $BiVO_4$ film, in the Na_2SO_4 electrolyte, is about twice the value of the higher current measured in the KCl electrolyte, suggesting that charge recombination is partially suppressed by fast hole oxidation of these substrates in different electrolytes. The higher photogenerated current in Na_2SO_4 electrolyte, when compared to NaCl, may be related to easier oxidation of sulfate group (SO_4^{-2}) when compared to water and chloride ions (Cl^-) in the applied potential window (0–1.4 V) [38]. The results shown here, concerning the high photocurrent in Na_2SO_4 electrolyte, are in good agreement with previous reports for $BiVO_4$ films obtained by other techniques [39, 40]. For instance, Kho and coworkers [41] analyzed $BiVO_4$ films deposited on ITO substrate by spray pyrolysis and the cyclic voltammetry results in Na_2SO_4 solution at 0.8 V vs. Ag/AgCl show a photoinduced current

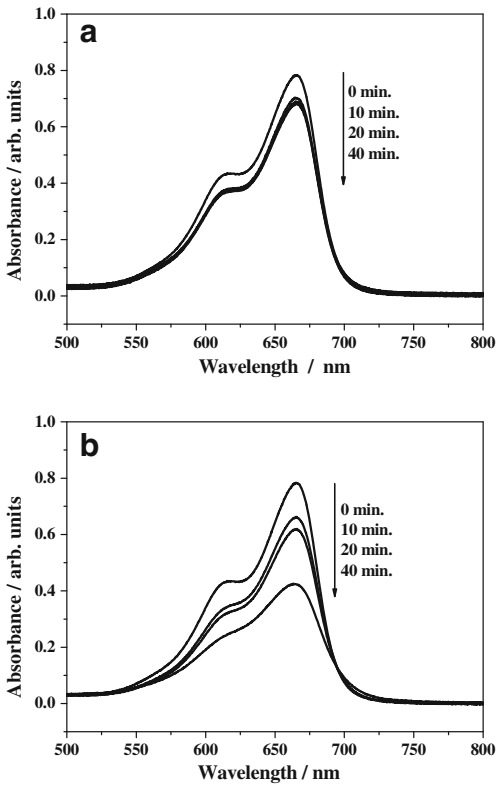

Fig. 6 UV–Vis optical absorption spectra of methylene blue solution by the $BiVO_4$ thin film. **a** After electrochemical degradation. **b** After photoelectrochemical degradation

Table 1 Kinetic parameters for methylene blue degradation

Electrodes	Kinetic parameters	
	k_{obs}/ min	Degradation % at 40 min
$BiVO_4$/FTO (dark)	0.003	13
$BiVO_4$/FTO (light)	0.015	46

density of 3 μA cm^{-2}. Under practically the same experimental conditions, except the substrate, which in our case is FTO, the photogenerated current density is of the same magnitude, and in our case, it is rather higher, about 5 μA cm^{-2}.

Photoelectrochemical degradation of methylene blue

Figure 6 shows UV–Vis absorption spectra of the methylene blue solution after electrochemical degradation (Fig. 6a) and after photoelectrochemical degradation (Fig. 6b) with the $BiVO_4$ films. The photoelectrochemical degradation of the $BiVO_4$ thin film was done by chronoamperometry, with a controlled potential of 1.4 V vs. Ag/AgCl, under visible light irradiation. Previously to light irradiation, the degradation of methylene blue was carried out in the dark, with the same applied potential. In this case, the film has shown as electroactive, degradating about 13 % of methylene blue in 40 min, as can be inferred from the UV–Vis spectra shown in Fig. 6a, where the maximum absorption at 665 nm is used as an evaluation parameter for degradation, recalling that the optical absorption of methylene blue at 665 nm is related to solution discoloration, caused by $OH^{\bullet}$ radical attack, formed at films surface, to molecule chromophore groups. Under light influence, the degradation has reached 46 % evaluated at 40 min. It has been reported that both forms of degradation, electrochemical as well as photoelectrochemical, are more efficient when compared to photocatalytic process [15], where the catalyst is in the form of powder, dispersed in the material to be degradated. This higher efficiency of the photoelectrochemical compared to photocatalytic is attributed to the combination of the effect of visible light irradiation with the applied potential in the films, which is not possible when the catalyst is in the form of powder. The light incidence increases the charge carrier generation and the applied bias forces the photogenerated electrons to flow towards the counter-electrode, preventing the fast electron hole recombination-back process. Then, the surface-photogenerated holes in the $BiVO_4$ film lead to the methylene blue oxidation with higher efficiency.

Figure 7 shows the decrease in methylene blue concentration as a function of reaction time. The inset in Fig. 7 shows the degradation percentage for a fixed time around 40 min, comparing both processes. As already mentioned, the photoelectrochemical process shows higher efficiency for the degradation by the $BiVO_4$ film, when compared to the dark procedure. The decay profile of the curves suggests that both processes follow first-order kinetics. The rate constant of the reaction (k_{obs}) can be evaluated by Eq. 1 [42]:

$$\ln(\mathrm{Abs_t}/\mathrm{Abs_o}) = -k_{obs}t \quad (1)$$

where Abs_o and Abs_t correspond to the methylene blue optical absorption before and after the reaction, respectively, and t is the reaction time. The kinetic parameters, rate constant and degradation percentage, are summarized in Table 1. The rate constant of the photoelectrochemical degradation reaction by the $BiVO_4$ film is about 15×10^{-3} min^{-1}, which is approximately five times the rate constant for electrochemical degradation (about 3×10^{-3} min^{-1}).

Conclusions

DTA/TGA curves of the precursor green gel along with X-ray diffraction data of thin films show that the SCS technique coupled to the dip-coating process is an efficient tool for obtaining monoclinic phase of $BiVO_4$ thin films. SEM images show that the thermal annealing time is fundamental in order to get homogenous thickness and particle distribution. When the time is appropriately controlled, the film is composed of a uniform distribution of round-shaped grains. UV–Vis optical absorption data of thin films reveal a direct bandgap transition of about 2.5 eV, typical of the monoclinic phase of $BiVO_4$.

The thin film voltammetry profile shows a good performance of the $BiVO_4$ in Na_2SO_4 electrolyte, with about twice higher photocurrent, when compared to KCl electrolyte. The photoelectrochemical degradation of methylene blue by $BiVO_4$ films leads to a rate constant five times higher than the electrochemical degradation carried out in the dark.

The results shown in this paper are a very good indication that the SCS/dip-coating technique combination is very adequate for obtaining the direct bandgap $BiVO_4$ semiconductor. Besides, it can be stated that this compound in the form of thin film presents a high potential application for the degradation of organic pollutants in aquatic environments.

Acknowledgments The authors wish to thank Prof. Margarida J. Saeki for the SEM images. They also acknowledge CNPq, FAPESP, and Fundação Araucaria (15585/2010) for financial support.

References

1. Akihiko K, Yugo M (2009) Chem Soc Rev 38:253–278
2. Rajeshwar K, de Tacconi NR (2009) Chem Soc Rev 38:1984–1998
3. Xie B, He C, Cai P, Xiong Y (2010) Thin Solid Films 518:1958–1961
4. Fujishima A, Honda K (1972) Nature 238:37–38
5. Lim AR, Lee KH, Choh SH (1992) Solid State Commun 83:185–186
6. Hirota K, Komatsu G, Yamashita M, Takemura H, Yamaguchi O (1992) Mater Res Bull 27:823–830
7. Tucks A, Beck HP (2007) Dyes Pigm 72:163–177
8. Zhang A, Zhang J (2009) Spectrochimica Acta Part A 73:336–341
9. Yin WZ, Wang WZ, Shang M, Zhou L, Sun SM, Wang L (2009) Eur J Inorg Chem 2009:4379–4384
10. Dunkle SS, Helmich RJ, Suslick KS (2009) J Phys Chem C 113:11980–11983
11. Long MC, Cai WM, Kisch H (2008) J Phys Chem C 112:548–554

12. Sayama K, Nomura A, Arai T, Sugita T, Abe R, Yanagida M, Oi T, Iwasaki Y, Abe Y, Sugihara H (2006) J Phys Chem B 110:11352–11360
13. Kudo A, Ueda K, Kato H, Mikami I (1998) Catal Lett 53:229–230
14. Walsh A, Yan Y, Huda MN, Al-Jassim MN, Wei SH (2009) Chem Mater 21:547–551
15. Zhou B, Qu J, Zhao X, Liu H (2011) J Environ Sci 23:151–159
16. Tokunaga S, Kato H, Kudo A (2001) Chem Mater 13:4624–4628
17. Jiang H, Endo H, Natori H, Nagai M, Kobayashi K (2009) Mat Res Bull 44:700–705
18. Lim AR, Choh SH, Jang MH (1995) J Phys Condens Matter 7:7309–7323
19. Yu J, Kudo A (2006) Ad Funct Mater 16:2163–2169
20. Zhang L, Chen D, Jiao X (2006) J Phys Chem B 110:2668–2673
21. Zhou L, Wang W, Liu S, Zhang L, Xu H, Zhu W (2006) J Mol Catal A: Chem 252:120–124
22. Yu J, Zhang Y, Kudo A (2009) J Solid State Chem 182:223–228
23. Zhou L, Wang W, Zhang L, Xu H, Zhu W (2007) J Phys Chem C 111:13659–13663
24. Dall'Antonia LH, de Tacconi NR, Chanmanee W, Timmaji H, Myung N, Rajeshwar K (2010) Electrochem Solid State Lett 13:D29–D32
25. Liu H, Nakamura R, Nakato Y (2005) J Electrochem Soc 152: G856–G861
26. Timmaji HK, Chanmanee W, de Tacconi NR, Rajeshwar K (2011) J Adv Oxid Technol 14:95–105
27. Zhang X, Chen S, Quan X, Zhao H (2009) Sep Pur Technol 64:309–313
28. Zhang X, Quan X, Chen S, Zhang Y (2010) J Hazard Mater 177:914–917
29. Jiang HQ, Endo H, Natori H, Nagai M, Kobayashi K (2008) J Eur Ceram Soc 28:2955–2962
30. Li M, Zhao L, Guo L (2010) Int J Hydrogen Energy 35:7127–7133
31. Pérez UMG, Sepulveda-Guzman S, Cruz AM, Méndez UO (2011) J Mol Catal A: Chem 335:169–175
32. Toulboul M, Vachon C (1988) Thermochim Acta 133:61–66
33. Cullity BD, Stock SR (2001) Elements of X-ray diffraction. Prentice Hall, New Jersey
34. Li G, Zhang D, Yu JC (2008) Chem Mater 20:3985–3989
35. Bhattacharya AK, Mallick KK, Hartridge A (1997) Mat Lett 30:7–13
36. Wang F, Shao M, Cheng L, Hua J, Wei X (2009) Mat Res Bull 44:1687–1691
37. Zhang X, Ai Z, Jia F, Zhang L, Fan X, Zou Z (2007) Mat Chem Phys 103:162–167
38. Berglund SP, Flaherty DW, Hahn NT, Bard AJ, Mullins CB (2011) J Phys Chem C 115:3794–3802
39. Su J, Guo L, Bao N, Grimes CA (2011) Nano Lett 11:1928–1933
40. Luo H, Mueller AH, McCleskey TM, Burrell AK, Bauer E, Jia QX (2008) J Phys Chem C 112:6099–6102
41. Kho YK, Teoh WY, Iwase A, Mädler L, Kudo A, Amal R (2011) Appl Mater Interfaces 3:1997–2004
42. Zhou Y, Vuille K, Heel A, Probst B, Kontic R, Patzke GR (2010) Appl Catal A 375:140–148